# Estimation of Acoustic Properties, of the Representative Volume Element of Random Fibrous Media

Charles Peyrega, Dominique Jeulin

AIP | Journal of Applied Physics

# Estimation of acoustic properties and of the representative volume element of random fibrous media

Charles Peyrega and Dominique Jeulin

Citation: J. Appl. Phys. **113**, 104901 (2013); doi: 10.1063/1.4794501
View online: http://dx.doi.org/10.1063/1.4794501
View Table of Contents: http://jap.aip.org/resource/1/JAPIAU/v113/i10
Published by the American Institute of Physics.

JOURNAL OF APPLIED PHYSICS **113**, 104901 (2013)

# Estimation of acoustic properties and of the representative volume element of random fibrous media

Charles Peyrega[a] and Dominique Jeulin[a]
*Centre de Morphologie Mathématique, Mathématiques et Systèmes, Mines ParisTech, 35 rue Saint Honoré, 77300 Fontainebleau, France*

(Received 10 July 2012; accepted 21 February 2013; published online 11 March 2013)

This work focuses on the estimation of acoustic properties from numerical simulations, and on the determination of the representative volume element of random fibrous media. At the microscopic scale, both viscous and thermal dissipations of energy occur in the air saturating the pores of a porous medium. Thus, the thermoacoustic formalism was used to model the physical behavior of several periodic unit cells of random fibrous media. Their properties such as both harmonic acoustic velocity and temperature were homogenized at different scales, in order to estimate representative volume elements for different properties. © *2013 American Institute of Physics*. [http://dx.doi.org/10.1063/1.4794501]

## I. INTRODUCTION

For engineering purpose, predicting acoustic properties of random media from their microstructure is a first step to design new materials with improved properties, like a better sound attenuation. One of the challenging problems to solve concerns the fluctuations of the microstructure and of the local physical fields involved in the homogenization of the acoustic behaviour.

This work was inspired by previous studies made in the framework of the Silent Wall project, with a main objective, which consisted in designing an insulating system using fibrous media with optimized acoustic absorption properties. Several results are available in previous publications (Refs. 32–34) and will not be detailed in this paper. The main method, we used to estimate the acoustic behaviour of fibrous media was based on finite element simulations over periodic unit cells of regularly distributed parallel fibres. This paper focuses on the acoustic absorption properties of fibrous media composed of randomly distributed fibres, in order to estimate the characteristic sizes of the simulated acoustic fields. Finally, the main objective of this work consists in defining the representative volume element of such random cells to estimate the coefficient of acoustic absorption with a controlled statistical precision.

## II. MODELLING THERMOACOUSTICS

### A. The thermoacoustic equations

Our work highlights the macroscopic properties of fibrous media from their behaviour at the microscopic scale, by simulating their thermo-acoustic properties, in order to correctly handle the viscous and thermal dissipation of the acoustic energy.[14,21,28,32,41] Starting from three harmonic variables: the flow velocity $\vec{U}$ (Eq. (1)), the pressure P (Eq. (2)), and the temperature of the fluid $T$ (Eq. (3)), we consider their variations, respectively, defined as acoustic velocity $\vec{u}$, pressure $p$, and temperature $\tau$.

$$\vec{U} = \vec{U_0} + \vec{u}\, e^{i\omega t}, \tag{1}$$

$$P = P_0 + p\, e^{i\omega t}, \tag{2}$$

$$T = T_0 + \tau\, e^{i\omega t}. \tag{3}$$

Four fully coupled equations are solved: the equation of Navier Stokes (Eq. (4)), the equation of continuity (Eq. (5)), the heat equation (Eq. (6)), and finally the equation of the perfect gases (Eq. (7)) inside the pores saturated by air. The air is considered as a visco-thermal fluid and as a perfect gas at the microscopic scale. The ambient pressure and temperature are, respectively, defined as $P_0$ and $T_0$.

$$i\,\omega\,\rho_0\,\vec{u} = -\vec{\nabla}p + \left(\frac{\eta}{3} + \zeta\right)\vec{\nabla}(\vec{\nabla}.\vec{u}) + \eta\,\Delta\vec{u}, \tag{4}$$

$$i\,\omega\,\frac{\rho}{\rho_0} + \vec{\nabla}.\vec{u} = 0, \tag{5}$$

$$i\,\omega\,\rho_0\,Cp\,\tau = \kappa\,\Delta\tau + i\,\omega\,p, \tag{6}$$

$$\rho(p,\tau)|_{P_0,T_0} = \rho_0\left(\frac{p}{P_0} - \frac{\tau}{T_0}\right). \tag{7}$$

Moreover, our study is made in the framework of the formalism proposed by Refs. 1, 3, and 18, which considers a porous medium as an equivalent fluid with a rigid skeleton (here the fibrous network). Thus, the interface $\Gamma$ between fibres and pores is considered as an adiabatic rigid boundary, which implies both acoustic velocity $\vec{u}$ (Eq. (8)) and temperature $\tau$ (Eq. (9)) equal to zero on $\Gamma$.

$$\vec{u}_\Gamma = \vec{0}, \tag{8}$$

$$\tau_\Gamma = 0. \tag{9}$$

[a]Electronic mail addresses: Charles.Peyrega@mines-paristech.fr and Dominique.Jeulin@mines-paristech.fr. URL: http://cmm.ensmp.fr/.

 

### B. Homogenization of periodic structures in acoustics

In order to estimate, the macroscopic acoustic properties of a porous medium from its physical behaviour at the microscopic scale, we use the theory of the homogenization of periodic structures.[5–7,39,40] This method was handled in our previous work concerning the thermoacoustic modelling of fibrous media (Refs. 32–34), and was inspired from different studies concerning different porous materials (Refs. 15, 21, 22, 28, 30, 37, and 41).

The three complex acoustic variables $\vec{u}$, $p$, and $\tau$ are $\Omega - periodic$ on the boundaries $\Gamma$ of the cells defined into the domain $\Omega$. According to this method these three variables can be expressed from a multi-scale point of view.[15,21,22,28–34,41,42] Considering a periodic microscopic unit cell $\Omega$, it is possible to estimate the acoustic absorption of the corresponding fibre board from the effective tensor of dynamic viscous permeability $\mathbf{K}$ and from the effective scalar thermal permeability $K'$ of this cell, assuming that viscous and thermal phenomena can be handled separately.[1,3,8–10,12,18,20,25–27,38,44] The local values of $\mathbf{K}$ and $K'$ in the microscopic cell are, respectively, estimated from the Eq. (10) (the Darcy's law) and the Eq. (11).

$$\overrightarrow{u^{(0)}}(\vec{x},\vec{y}) = -\frac{\boldsymbol{K}(\vec{y},\omega)}{\eta}.\overrightarrow{\nabla_x} p^{(0)}(\vec{x}), \tag{10}$$

$$\tau^{(0)}(\vec{x},\vec{y}) = \frac{K'(\vec{y},\omega)}{\kappa}\, i\,\omega\, p^{(0)}(\vec{x}). \tag{11}$$

As explained in Refs. 18, 20–22, and 38, the multiscale approach links the macroscopic and the microscopic acoustic properties of our fibrous medium, respectively, characterized by two spatial variables noted $x$ and $y$. Thus, from a separation of scales, we note $\overrightarrow{\nabla_x} p(x)$ the gradient of the macroscopic pressure in the material which is assumed to be constant at the microscopic scale.[21,22] Therefore, the acoustic pressure is assumed to be a macroscopic variable only depending on the macroscopic spatial variable $x$. We can notice that both $\mathbf{K}$ and $K'$ are locally defined at the microscopic scale $y$ and depend on the frequency $\Omega$ of the acoustic propagating wave. Let for instance $p(x) = 1\,Pa$ be the constant amplitude of the macroscopic acoustic pressure applied to the fibrous material.

### C. Macroscopic acoustic properties of homogenized porous media

As an illustration for this method, we first consider in Fig. 1 an infinite layer in 3D having a thickness equal to $d$. This layer is composed of a periodic pattern of parallel regularly distributed fibres (called PACC: periodic array of circular cylinders, according to Ref. 41), and is stimulated by an incoming propagating acoustic wave, which splits into a reflected wave and an absorbed wave. In our work our objective consists in optimizing the acoustic properties of such a medium by increasing the fraction of the incoming wave absorbed by the material.

Let $\mathbf{K}$ and $K'$, respectively, be the effective viscous permeability and the effective thermal permeability of the full

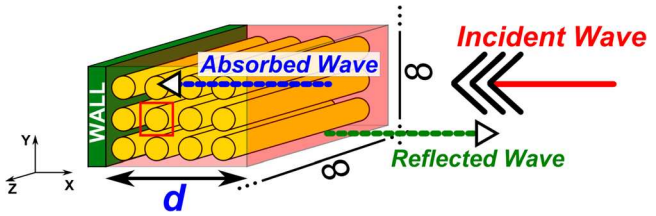


FIG. 1. 3D equivalent infinite layer (along $Oy$ and $Oz$) of homogenized material composed of elementary periodic unit cells PACC (fibres with circular cross section) having a thickness equal to $d$ along $Ox$. Stimulation along $Ox$. Red square: 2D unit cell (Fig. 2).

$\Omega$ unit periodic cell Fig. 2 (i.e., over both porous and fibrous phases).

In order to estimate, the acoustic properties of such a fibrous medium, we solved the thermoacoustic equations presented in Sec. II A with the finite element software Comsol Multiphysics™,[11] for different frequencies between 0 Hz and 4032 Hz. Only the pores around the rigid fibre are meshed into Fig. 2, but we consider both Eqs. (8) and (9) in the fibrous phase (central white disc). Moreover, the mesh at the interface $\Gamma$ was refined in order to properly solve the equations in the boundary layer (more details are given in Sec. II D)). We note $\boldsymbol{\rho_{eff}}$ the effective tensor of density of the macroscopic equivalent medium, which is estimated by below equation

$$\boldsymbol{\rho_{eff}} = \frac{\eta\,\phi}{i\,\omega}\boldsymbol{K}^{-1}. \tag{12}$$

Then, we estimate the effective scalar compressibility modulus $\chi_{eff}$ (Eq. (13)), with $Pr$ the Prandtl number of the air, and $\gamma = 1.4$, the perfect gas constant.

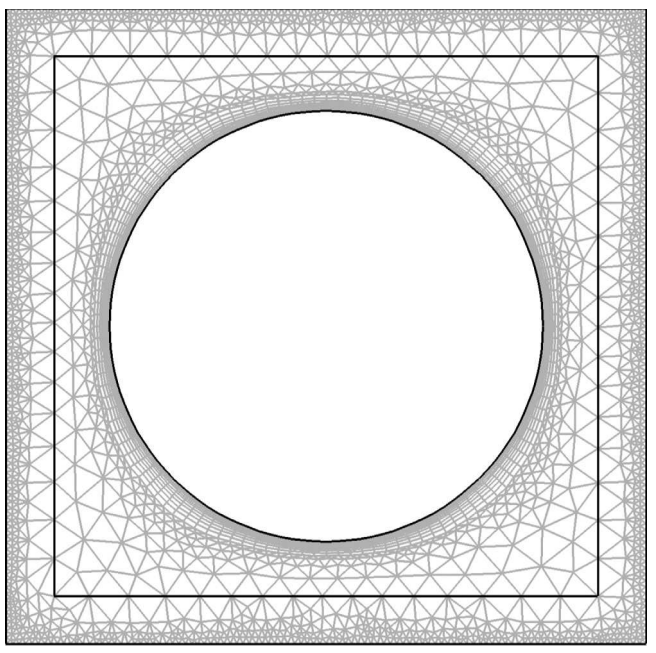

FIG. 2. 2D PACC 64 meshed periodic unit cell representing a cross section of the geometry in Fig. 1. Only the pores are meshed with a porosity $\Phi = 0.64$.

$$\chi_{eff}(\omega) = \frac{1}{\gamma P_0}\left(\gamma - \left[(\gamma - 1)\frac{\rho_0 Pr}{\eta}\frac{i\omega K'}{\phi}\right]\right). \quad (13)$$

Considering $\vec{Q} = Q\vec{\xi}$ the wave vector defined from the unit vector $\vec{\xi}$ and parameters $\rho_{eff}$ and $\chi_{eff}$, we can estimate the effective characteristic velocity $\boldsymbol{c_{eff}}$ (Eq. (14)) and the effective characteristic acoustic impedance $Zc_{eff}$ (Eq. (15)) of the homogenized porous medium.

$$c_{eff} = \sqrt{\frac{\overrightarrow{\xi^T}\,\boldsymbol{\rho_{eff}}^{-1}\,\vec{\xi}}{\chi_{eff}}} = \frac{\omega}{Q}, \quad (14)$$

$$Zc_{eff} = \frac{1}{\phi}\sqrt{\frac{\overrightarrow{\xi^T}\,\boldsymbol{\rho_{eff}}\,\vec{\xi}}{\chi_{eff}}}. \quad (15)$$

Finally, parameters $\rho_{eff}$ and $\chi_{eff}$ can be used to calculate the acoustic impedance $Z_d$ (Eq. (16)) of a macroscopic medium having a thickness equal to $d$ (Fig. 1).

$$Z_d = Zc_{eff}\left[\frac{1 + e^{\left(\frac{-2i\omega d}{c_{eff}}\right)}}{1 - e^{\left(\frac{-2i\omega d}{c_{eff}}\right)}}\right]. \quad (16)$$

The coefficient of reflection $R(\omega)$ (Eq. (17)) is a complex number estimated from $Z_d$ and from $Z_0 = \rho_0 c_0$, the impedance of the air saturating the pores, and leads to the coefficient of absorption $A(\omega)$ (Eq. (18)) of the corresponding d-thick macroscopic material.

$$R(\omega) = \frac{Z_d - Z_0}{Z_d + Z_0}, \quad (17)$$

$$\alpha(\omega) = 1 - |R(\omega)|^2. \quad (18)$$

### D. Macroscopic acoustic properties of deterministic fibrous media

In previous works, using image processing methods like mathematical morphology (Refs. 32, 35, and 36), we have highlighted some morphological properties of the Thermisorel™ at the microscopic scale, such as its external porosity $\Phi = 0.64$ and its volume weighted average radius $R_F = 42\,\mu$m. The 3D microstructure of this fibrous material is illustrated in Fig. 3 with a 3D tomographic X-Ray image. In the further experimental results concerning the Thermisorel™, the acoustic stimulation is made along the $Oz$ axis, perpendicularly to the fibres which are isotropically oriented in the $xOy$ planes.

For instance, Fig. 4 shows that a 4 cm thick fibre board like the Thermisorel™ (black and green plots) has a similar acoustic absorption coefficient as the simulated deterministic medium composed of 2D PACC 64 periodic unit cells (Fig. 2) with a radius equal to $R_F = 42\,\mu$m (orange plot), in the frequency range between 53 Hz and 4032 Hz. Note that the homogenized acoustic absorption coefficient is obtained without any experimental fitting from measurements. The experimental acoustic absorption of the Thermisorel™ was measured by the LAUM (Laboratoire d'Acoustique de l'Université du Maine, Le Mans, France) with a Kundt's tube.

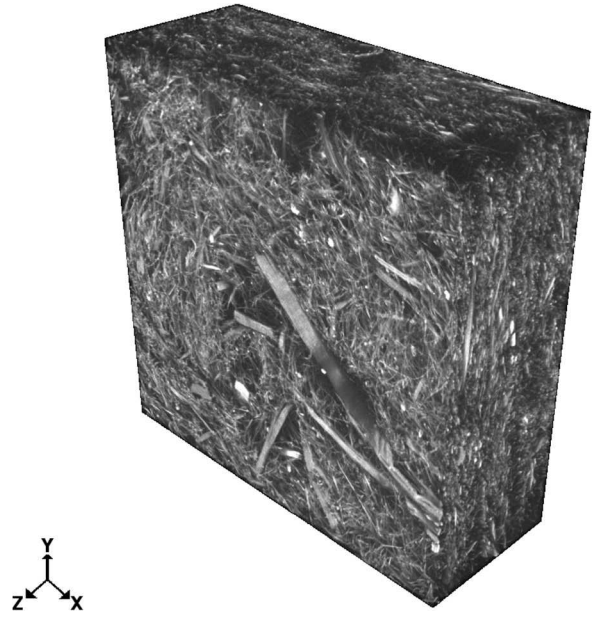


FIG. 3. 3D X-Ray CT image of Thermisorel™. Resolution: 15$\mu$m/*voxel*.

Note that the two peaks of absorption around 2500 Hz in Fig. 4 are measurement artefacts due to the vibration resonances of the Kundt's tube used to measure $\alpha(\omega)$, and therefore are not significant. In Fig. 4, we can observe to what extent the size of the fibre radii influences the absorption coefficient of a fibre board with a given porosity (here $\Phi = 0.64$) and thickness (here $d = 4$ cm).

These results are more detailed in our previous publications on this topic (Refs. 32–34), where it was shown to what extent a compromise should be found between small and large fibres. Decreasing the radius of the fibres for a given porosity $\Phi$ implies an increase of the specific surface area $S_v$ of the fibres-pores interface, expressed in $m^{-1}$. According to

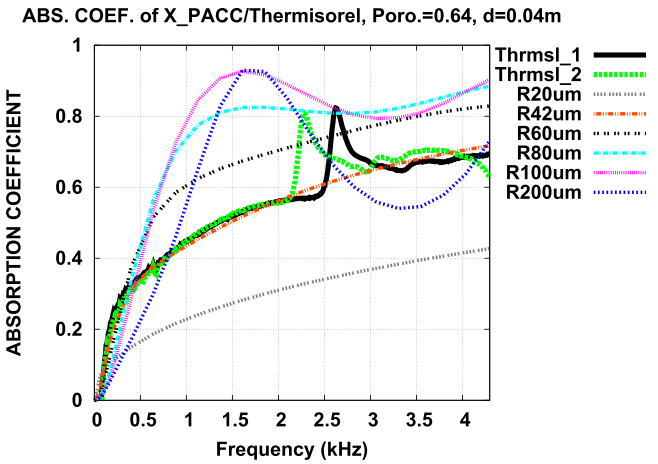


FIG. 4. Acoustic absorption coefficients of single layered materials composed of 2D PACC cells with a porosity $\Phi = 0.64$, for different fibre radii, and having a thickness $d$ equal to 4 cm, for $f$ between 53 Hz and 4032 Hz. Comparison to the experimental properties of Thermisorel™ (Source: LAUM).

the Eq. (19), the specific surface area is the ratio between the surface of the fibres-pores interface $S$ and the total volume of the sample.

$$S_v = \frac{S}{V_{Total}}. \tag{19}$$

In acoustics, the dissipation of energy occurs at this interface, in the so-called boundary layer, whose thickness $\delta_{BL}$ is directly linked to the frequency of the propagating sound wave, according to the Eq. (20).[1,2] Thus, the lower the frequency the thicker the boundary layer. That is, why the finite element mesh of the microstructures has to be refined at the interface of the fibres (Fig. 2), in order to properly resolve the thermoacoustic equations in the boundary layer, and then to correctly estimate the acoustic properties of the cell.

$$\delta_{BL} = \sqrt{\frac{\eta}{f\,\pi\,\rho_0}}. \tag{20}$$

Knowing the relationship between the thickness $\delta_{BL}$ and the frequency $f$, we observed that reducing the radius $R_F$ implies an increasing surface area $S_v$ for a given pore volume fraction, and then a global increasing acoustic absorption in the frequency range (cf. plots for $R_F = 200\,\mu$m (blue plot) and $R_F = 100\,\mu$m (pink plot) in Fig. 4). However, reducing the size of the fibres too much, with a constant pore volume fraction $\Phi$, will cause an observable drop of the acoustic absorption coefficient (cf. plots for $R_F = 80\,\mu$m (black dashed plot) to $R_F = 20\,\mu$m (gray dashed plot) in Fig. 4).

## III. RANDOM FIBROUS MEDIA

### A. Acoustic fields simulated on random unit cells

In the Sec. II C was introduced a computational method to simulate the thermoacoustic behaviour of a deterministic fibrous medium. In this section, we will focus on the acoustic properties of random fibrous media, since the microstructure of the Thermisorel™ is heterogeneous. In previous publications, a morphological model was proposed to represent 3D virtual fibrous materials with morphological properties similar to the Thermisorel™. Based on the theory of random sets (Refs. 16 and 23), our method makes use of a Boolean model of random cylinders with random radii, lengths and orientations in 3D.[32,35] Since the theoretical morphological properties of the random Boolean model are known, it is possible to make an identification of the model from image analysis measurements.

In this study, we have chosen to model random fibrous media by infinite parallel fibres, like 2D PACC cells in Fig. 1, but randomly distributed in 3D, with cross sections representing a Boolean model of discs. We will call these geometries 2D PACC RANDOM. The Fig. 5 shows the static fields of acoustic velocity in two unit cells (1 and 2) among $n = 20$ independent realizations, composed of overlapping fibres in accordance with the Boolean model, as the result of the location of the centres of discs, according to a random Poisson point process.[16,23] These unit cells $\Omega$ are $\Omega - periodic$, which

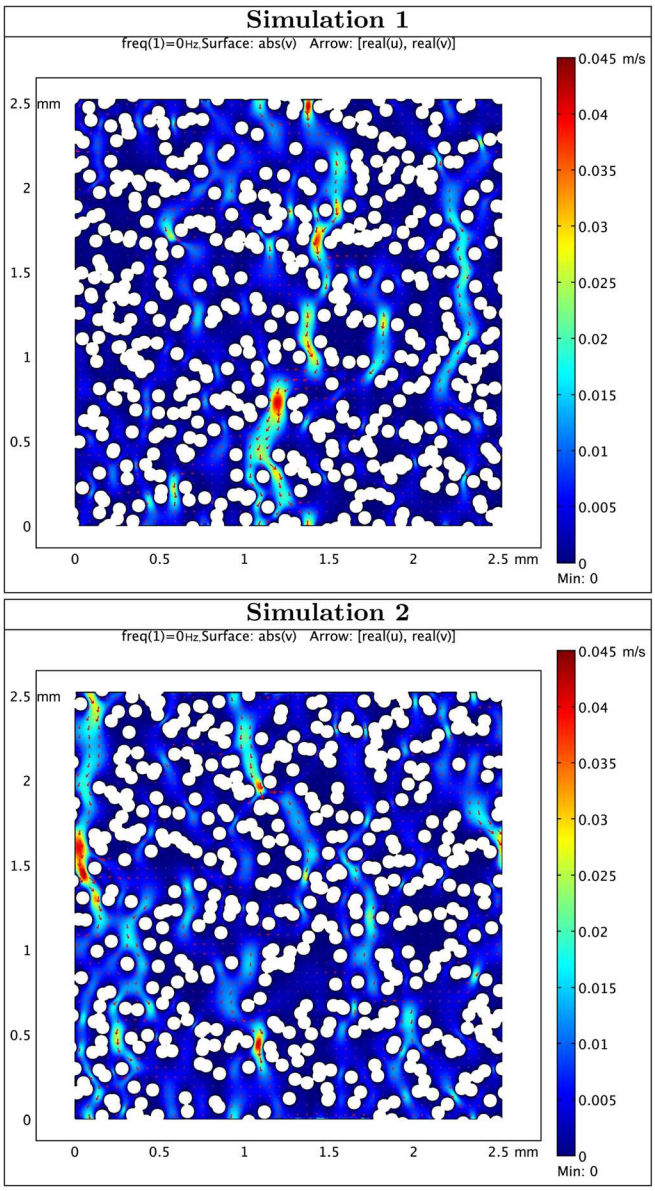


FIG. 5. Static fields of acoustic velocity $\vec{u}$ (m/s) (f = 0 Hz) for two periodic elementary unit cells (among 20 independent realizations). Acoustic stimulation in the vertical $Oy$ direction, sources at the top of the geometries. $R_F = 42\,\mu$m.

means that the three acoustic fields $\vec{u}$, $p$, $\tau$, and even the geometries of their microstructures, are periodic in both $Ox$ and $Oy$ directions. Moreover, all the fibres have the same radius (here $R_F = 42\,\mu$m).

Their pore volume fractions are respectively equal to $\Phi_A = 0.65$ and $\Phi_B = 0.66$. This fluctuation is a result of the Poisson point process driving the Boolean model (Refs. 23, 32, and 35) which implies random pore volume fractions around the average value $\Phi_{AVG} = 0.64$. This study is different from our previous work concerning the acoustic properties of random fibrous media (Refs. 32 and 34) because the considered microstructures were especially chosen for having a constant pore volume fraction (0.64). Thus, only the effects of the geometrical fluctuations at constant porosity were studied.

The absolute value of the complex harmonic acoustic fields $|\tau|$ of the simulation 1 are represented in Fig. 6 for frequencies in the range 53 Hz–1126 Hz, at two different scales:

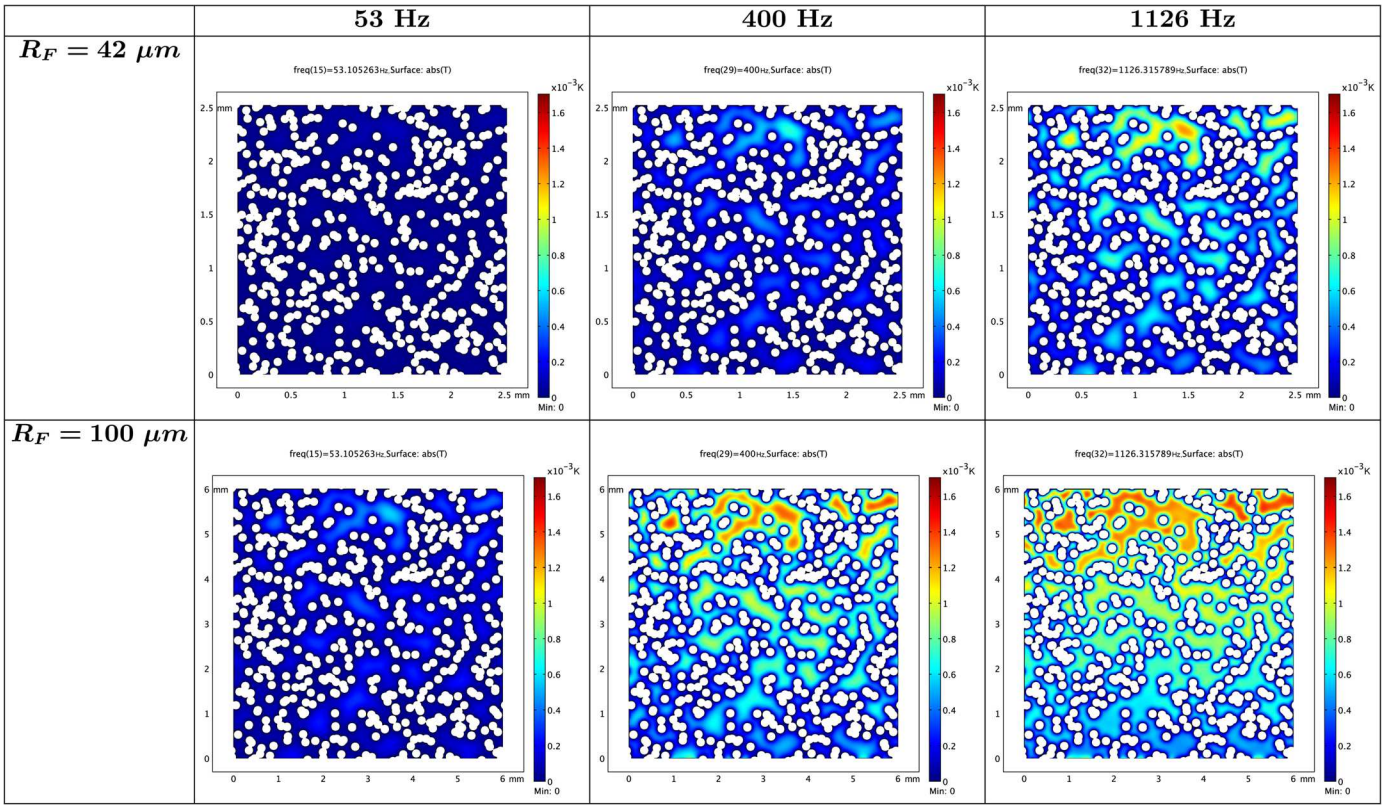


FIG. 6. Harmonic fields of acoustic temperature $\tau$ (K) for three frequencies $f$ between 53 Hz and 1126 Hz for the periodic elementary unit cell 1 at different scales ($R_F = 42\ \mu$m and 100 $\mu$m). Acoustic stimulation in the vertical $Oy$ direction, sources at the top of the geometries. In this illustration, the configuration of fibres is kept constant, while changing their diameter.

$R_F = 42\ \mu$m and 100 $\mu$m. Note that the square geometries at these two different scales are obtained with homothetic transformations, which are quantitatively described in the Table I, where the side lengths $l_C$ and surface areas $A_C$ of the 2D PACC RANDOM cells are listed for each scale of radius $R_F$.

Like in our previous work (Refs. 32–34), we can observe that the boundary layer (blue areas with $|\tau| \approx 0$ at the $\Gamma$ air-fibre interface) gets thinner at high frequency, and that an overlap of neighboring boundary layers is seen at low frequencies for small fibres.

Generally speaking, both acoustic fields $\vec{u}$ and $\tau$, respectively, represented in Figs. 5 and 6, are not homogeneous and local fluctuations appear. This directly influences the variations of the acoustic properties between realizations.

### B. Macroscopic acoustic properties of random fibrous media

After having simulated the thermoacoustic behaviour of $n = 20$ independent microstructures of periodic random fibrous media at three different scales $R_F = 42\ \mu$m, 100 $\mu$m, and 300 $\mu$m (which implies a total of $3 \times 20 = 60$ computational simulations), the next step consisted in estimating the average absorption coefficient $E\{\alpha(\omega)\}$ obtained from $n = 20$ independent realizations for each scale and for a given thickness (here $d = 2$ cm, 4 cm, and 10 cm). For each radius $R_F$, the average absorption coefficient in Fig. 7 was estimated from both permeabilities $E\{\boldsymbol{K}\}$ and $E\{K'\}$ averaged over the $n = 20$ independent periodic microstructures and injected in the equations in Sec. II C.

TABLE I. Lengths $l_C$ (in mm) and surface areas $A_C$ (in mm$^2$) of the 2D PACC RANDOM unit cells for the different fibre radii $R_F$ (in $\mu$m).

| $R_F$ | 42 $\mu$m | 100 $\mu$m | 300 $\mu$m |
|---|---|---|---|
| $l_C$ (mm) | 2.52 | 6 | 18 |
| $A_C$ (mm$^2$) | 6.35 | 36 | 324 |

In Fig. 7, the acoustic absorption of fibre boards composed of deterministic 2D PACC unit cells (in orange) are compared to the average absorption coefficient $E\{\alpha(\omega)\}$ (in green) obtained from the $n = 20$ 2D PACC RANDOM periodic microstructures for the case $d = 4$ cm, the conclusions derived from other thicknesses being similar. At first sight, we can observe that deterministic and random cells do not give exactly the same absorption coefficients, but they are close. For example, deterministic and random geometries with radii equal to $R_F = 42\ \mu$m have very similar acoustic absorption coefficients in the full frequency range. For larger fibres ($R_F = 100\ \mu$m and 300 $\mu$m) the frequency evolutions are globally similar with almost identical amplitudes, but a so-called "frequency shift" is observed between regular and random microstructures.

The blue dots in Fig. 7 represent the absorption coefficient of each experimental simulation (among $n = 20$). Thus, we can observe that for large fibres ($R_F = 300\ \mu$m), the fluctuations of the absorption coefficient are high.

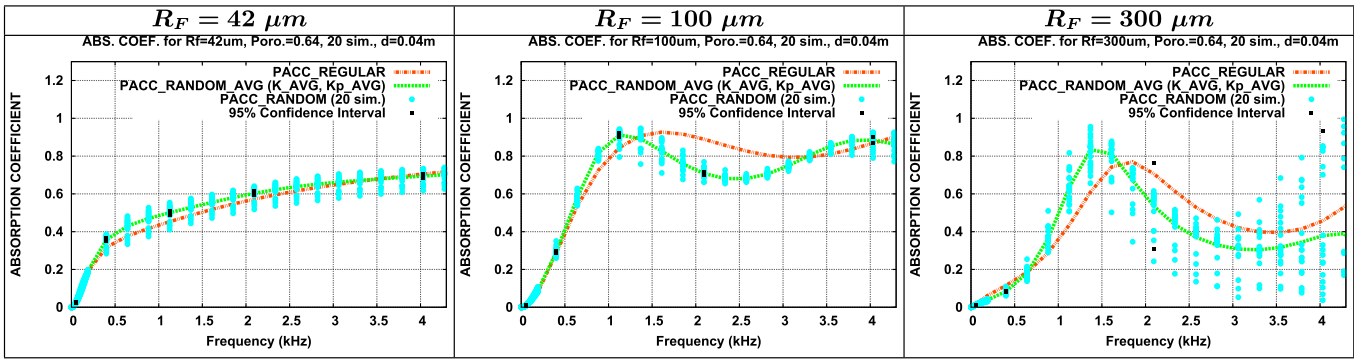


FIG. 7. Comparison of the absorption coefficient of regular 2D PACC 64 homogenized microstructures to the average absorption coefficient (in *green*) of the 20 independent homogenized random fibrous media (individual absorption in *blue*) having a thickness $d$ equal to 4 cm, for $f$ between 53 Hz and 4032 Hz. $R_F = 42\,\mu$m, 100 $\mu$m, and 300 $\mu$m.

## IV. ESTIMATION OF THE REPRESENTATIVE VOLUME ELEMENT

### A. General method

The fluctuations of $\alpha(\omega)$ observed throughout the $n = 20$ realizations in Fig. 7 can be quantified in order to define the relative precision $\epsilon$ to estimate the average absorption coefficient $E\{\alpha(\omega)\}$ over the $n = 20$ independent realizations, having a surface area $A_C$ (Table I).

In this section, we will present a method to estimate the representative volume element of such a material for different physical properties. The main objective consists in defining the minimum volume for which the properties remain stable, whatever the random sample considered. For this purpose the fluctuations of different acoustic fields (velocity, temperature, and absorption) are studied from $n$ independent unit cells composed of randomly distributed fibres.

In order to determine the relative precision $\epsilon$ of the estimation of an effective physical property $\langle Z\rangle$, obtained from $n$ independent random microstructures, each one having a surface area equal to $A_C$, it is necessary to estimate the variance $VAR(\langle Z\rangle)$ of the random variable $\langle Z\rangle$ over the $n$ independent unit cells. The relative precision $\epsilon$ is defined from the 95% estimation error $\epsilon_{95\%}$ (Eqs. (21) and (22)), deduced from the 95% confidence interval $\langle Z\rangle \pm \epsilon_{95\%}$ inside which the exact average value $E\{\langle Z\rangle\}$ is contained with a probability 0.95, $E\{\langle Z\rangle\}$ being the average of $\langle Z\rangle$ over the $n$ realizations of the cell.

$$\epsilon_{95\%}^2 = \frac{4 \times VAR(\langle Z\rangle_{A_C})}{n}, \tag{21}$$

$$\epsilon^2 = \frac{\epsilon_{95\%}^2}{E\{\langle Z\rangle\}^2}. \tag{22}$$

It is known (Refs. 4, 13, 17, 19, 24, and 43), that the variance $VAR(\langle Z\rangle)$ can be expressed by Eq. (23), as a function of the point variance $VAR(Z)$ and of the integral range $A_2$, namely the integral of the correlation function, as defined by Eq. (27) below, measuring the scale of the fluctuations of the average physical property $\langle Z\rangle$. Noting $A$ the surface area of the individual cells, we asymptotically obtain the Eq. (23) for $A \gg A_2$.

$$\frac{VAR(\langle Z\rangle_A)}{VAR(Z)} = A_2 \times \frac{1}{A}. \tag{23}$$

Thus, the relative precision of the estimation of $\langle Z\rangle$, obtained from $n$ independent unit cells with a surface area equal to $A = A_C$ (Eq. (24)), can be deduced from Eqs. (21)–(23) if the condition $A \gg A_2$ is satisfied.

$$\epsilon^2 = \frac{4 \times VAR(Z) \times A_2}{n \times A_C \times E\{\langle Z\rangle\}^2}. \tag{24}$$

In order to estimate the integral range $A_2$, the method we used consists in calculating the variance $VAR(\langle Z\rangle)$ of the average property $\langle Z\rangle$ over all the disjointed subareas $A$ of the domain $A_0 = n \times A_C$. Moreover, we note $VAR(Z)$ the point variance of the random property $Z$ over the total surface area $A_0$ of the $n$ microstructures. The use of Eq. (23) was validated in many previous studies (see Refs. 4, 13, 19, and 43, among others). A further validation is made here on the fluctuations of the area fraction, as explained at the end of Sec. IV B 1 and by comparison between theoretical and experimental results (Table II).

To illustrate this method, the Fig. 8 represents the effective acoustic velocity averaged over subareas of the microstructure 1 for different ratios (1, $\frac{1}{4}$, and $\frac{1}{9}$).

Finally, the representative volume element $A_{RVE_\epsilon}$, into which the average value $\langle Z\rangle$ of the random variable $Z$ is estimated with a relative precision $\epsilon$, is defined in Eq. (25).[4,13,17,19,43] The Eq. (25) is defined from the Eq. (24), with $n = 1$ and $A_2$ estimated from Eq. (23).

$$A_{RVE_\epsilon} = \frac{4 \times VAR(Z) \times A_2}{\epsilon^2 \times E\{\langle Z\rangle\}^2}. \tag{25}$$

### B. Representative volume element of the microstructure

#### 1. Integral range of the microstructure

Using the method presented in the Sec. IV A, we consider now as a random function $Z(x)$, the indicator function of the pores ($Z(x) = 1$ when $x$ is located inside the pores, and $Z(x) = 0$ in the fibres). In that case, the value $VAR(Z)$ in the

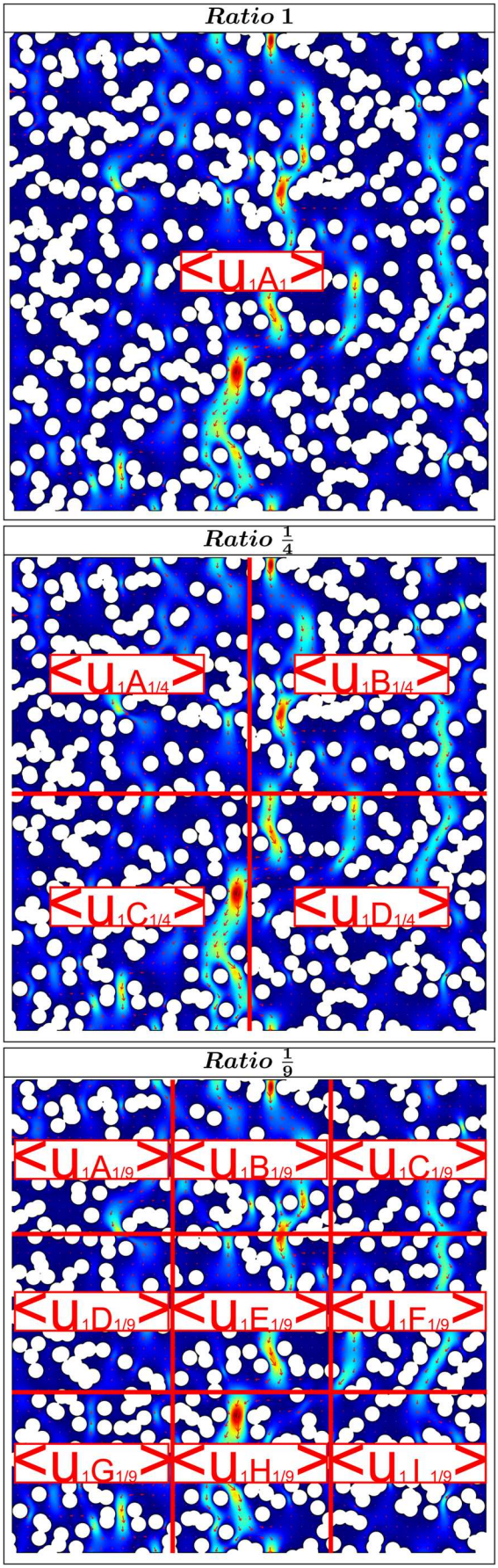


FIG. 8. Average acoustic velocity over subareas of the microstructure 1 for different surface ratios (1, $\frac{1}{4}$, and $\frac{1}{9}$). Acoustic stimulation in the vertical $Oy$ direction, source at the top of the geometry.

Eq. (23) is given by the equation: $VAR(Z) = \Phi \times (1 - \Phi)$, with $\Phi$ the area fraction of the pores.

Let $\bar{C}(h)$ be the centered covariance of a stationary random variable $Z$ with mathematical expectation $E\{Z\}$ (Eq. (26)).[24] We have

$$\bar{C}(h) = E\{(Z(x) - E\{Z\}) \times (Z(x+h) - E\{Z\})\}. \quad (26)$$

For the indicator function, we can write the following equation: $\bar{C}(h) = Q(h) - \Phi^2 = C(h) - (1-\Phi)^2$, with $C(h)$ and $Q(h)$ the covariances, respectively, of the fibres and of the pores. By definition, we have $C(h) = P\{x \in \text{fibres}, x+h \in \text{fibres}\}$, while $Q(h) = P\{x \in \text{pores}, x+h \in \text{pores}\}$. Then, the integral range $A_2$ can be obtained as a function of $\bar{C}(h)$ into the below equation

$$A_2 = \frac{1}{\Phi \times (1-\Phi)} \int_{\Re^2} \bar{C}(h) dh. \quad (27)$$

The random microstructures used for the simulations are Boolean models of random discs, which represent random fibrous media. They are obtained by implantation of discs with a random radius $R$ (here, we have $R = R_F$) on random points $x_k$ of a Poisson point process. Realizations of the model are shown on Figs. 5, 6, and 8, where it is clear that overlaps between discs are allowed, as a result of the Poisson point process, where points are located at random, without any interaction. Thus, $\bar{C}(h)$ can be analytically defined by the theoretical expression $Q_{BD}(h)$ of the covariance $Q(h)$ of the pores of a Boolean model of discs (noted $BD$) defined below.[16,23,32,35]

$$Q_{BD}(h) = \Phi^{(2-r_D(h))}. \quad (28)$$

We note $r_D(h)$, the normalized geometrical covariogram of a disc. The geometrical covariogram of any random primary grain $X'$ and its normalized geometric covariogram are respectively defined by the Eqs. (29) and (30), $\overline{\mu_n}$ being the average volume in 3D or the average area in 2D of the random grains $X'$, over the $n$ realizations.

$$K(h) = \overline{\mu_n}(X' \cap X_{-h}), \quad (29)$$

$$r(h) = \frac{K(h)}{K(0)} = \frac{K(h)}{\overline{\mu_n}(X')}. \quad (30)$$

Considering discs as primary grains having a constant radius $r$, we can note their geometrical covariogram as $K_D(h,r) = 0$ if $h > 2r$. It is obtained as the area of the intersection of two discs with the same radius $r$ when their centres are separated by distance $h$. The Eq. (31) gives by geometrical calculation the values of $K_D(h,r)$ when $0 \le h \le 2r$.

$$K_D(h,r) = 2r^2 \left( \arccos\left(\frac{h}{2r}\right) - \frac{h}{2r}\sqrt{1 - \left(\frac{h}{2r}\right)^2} \right). \quad (31)$$

Then, from Eqs. (28), (30), and (31) into the Eq. (27), it is possible to compute the theoretical integral range $A_{2_{BD}}$ of a Boolean model of random discs (Eq. (32)).

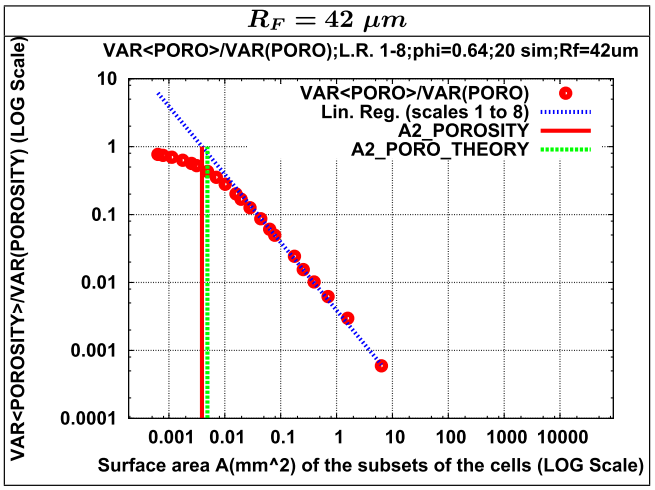


FIG. 9. Estimation of the integral range $A_2(Porosity)$ of $n = 20$ independent microstructures (Boolean model of random discs) for $R_F = 42\,\mu$m. Logarithmic scales.

$$\begin{cases} A_{2_{BD}} = \dfrac{4\pi}{VAR(Z)} \displaystyle\int_{h=0}^{2R_F} h\bar{C}_{BD}(h)\,\mathrm{d}h \\ A_{2_{BD}} = \dfrac{4\pi}{VAR(Z)} \displaystyle\int_{h=0}^{2R_F} h\left(Q_{BD}(h) - \Phi^2\right)\mathrm{d}h \\ A_{2_{BD}} = \dfrac{4\pi}{VAR(Z)} \displaystyle\int_{h=0}^{2R_F} h\left(\Phi^{\left(2-r_D(h)\right)} - \Phi^2\right)\mathrm{d}h. \end{cases} \tag{32}$$

Using the Eq. (23), the integral range $A_2$ of the microstructure (i.e., of the porosity) was estimated from a linear regression of the function $VAR(\langle\Phi\rangle_A)/VAR(\Phi)$ with respect to $(1/A)$. The function $VAR(\langle\Phi\rangle_A)$ was calculated by splitting the 20 realizations of 2D PACC RANDOM unit cells into equal disjointed subareas with different $A$ surface areas (Fig. 8). The Fig. 9 shows this linear regression over the scales 1 to 8 (i.e., over the surface ratios 1 to 1/64) in logarithmic scales for both axis for the case $R_F = 42\,\mu$m.

The resulting integral range $A_2$ is compared to the theoretical one (Eq. (24)) in the Table II. The theoretical values and the estimated values differ with a relative error close to 20% of the theoretical ones.

### 2. RVE of the porosity

After having estimated the integral range $A_2$ of the average porosity from $n = 20$ realizations in Sec. IV B 1 (Table II), we can estimate from the Eq. (25) the representative volume element $A_{RVE_\epsilon}$ for which the average porosity $\langle\Phi\rangle$ is known with the relative precision $\epsilon$. On the Fig. 10, is given the evolution of the relative precision of estimation $\epsilon$ of

TABLE II. Comparison between $A_{2_{Simu}}$ estimated over 20 microstructures, and the theoretical integral range $A_{2_{BD}}$ of an infinite Boolean model of random discs with a radius $R_F$.

| $R_F$ ($\mu$m) | $A_{2_{Simu}}$ (mm$^2$) | $A_{2_{BD}}$ (mm$^2$) |
|---|---|---|
| 42 | 0.0039 | 0.0049 |
| 100 | 0.0222 | 0.0277 |
| 300 | 0.1995 | 0.2495 |

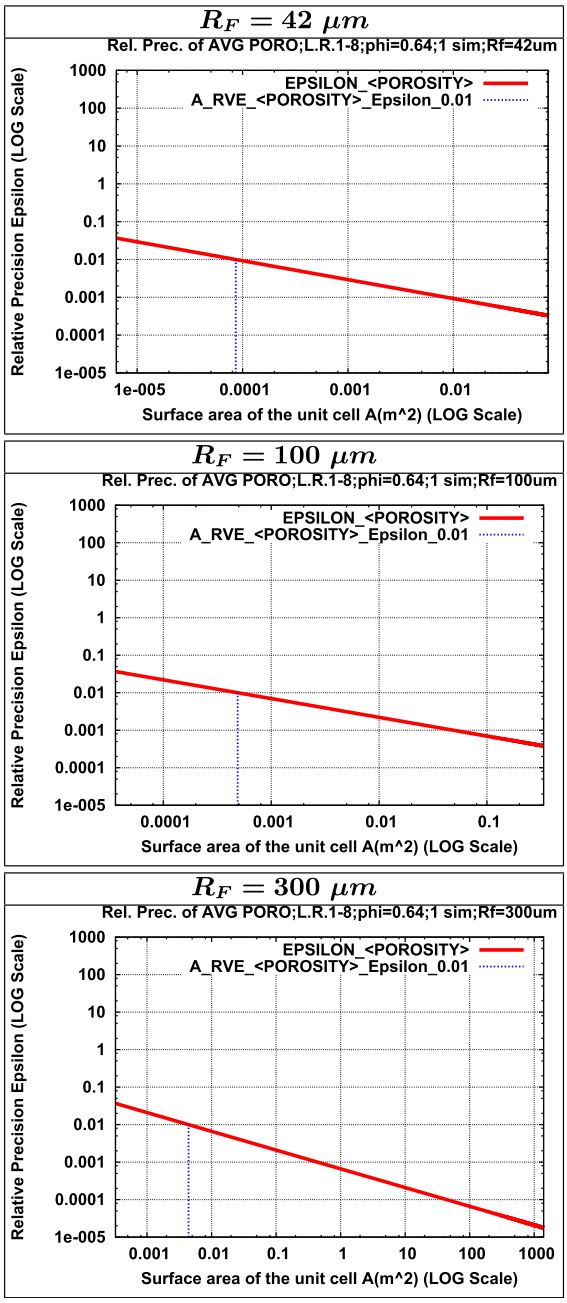


FIG. 10. Evolution of the relative precision of estimation $\epsilon$ of $\langle\Phi\rangle$ over the surface area $A$ of one random realization (n = 1) at different scales ($R_F = 42\,\mu$m, $100\,\mu$m, and $300\,\mu$m). The minimum surface area $A$ on the $Ox$ axis is equal to $A_C$ in Table I. Blue dashed vertical line: $\epsilon = 1$ %. Logarithmic scales.

$\langle\Phi\rangle$ as a function of the surface area $A$ of one random realization (n = 1) at different scales ($R_F = 42\,\mu$m, $100\,\mu$m, and $300\,\mu$m). It enables us to estimate the representative element $A_{RVE_\epsilon}$ for a specific precision $\epsilon$. The minimum surface area $A$ on the $Ox$ axis is equal to $A_C$ in Table I, which shows that a single realization like those simulated in our work provides an estimate $\langle\Phi\rangle$ with a relative precision $\epsilon_{\langle\Phi\rangle} = 3.7\%$.

According to the Eq. (24), the relative precision of the estimation of $\langle\Phi\rangle$ for the 20 images is equal to $\epsilon_{\langle\Phi\rangle} = 0.83\%$, which shows that both number ($n = 20$) and size ($A_C$) of images (Table I) are representative enough to estimate the average porosity $\langle\Phi\rangle$ with a very good precision. This conclusion is validated by the fact that the linear range for which

$A \gg A_2$ is relatively large in Fig. 9, since the linear regression of $VAR(\langle\Phi\rangle_A)/VAR(\Phi)$, according to $(1/A)$ was calculated over the 8 first area ratios (from 1 to 1/64).

### C. Representative volume element of complex acoustic fields

#### 1. Integral range of complex acoustic fields

Since both variables $\vec{u}$ and $\tau$ are complex, our study separately focuses on the respective real and imaginary parts of these two variables. Thus, the estimation of the RVE handles the following four fields: $Re[\vec{u}]$, $Im[\vec{u}]$, $Re[\tau]$, and $Im[\tau]$. Moreover, we consider the random scalar fields $Re[u_y]$, $Im[u_y]$, $Re[\tau]$, and $Im[\tau]$ as random functions. We note $u_y$ the scalar complex component of $\vec{u}$ along $Oy$, because the acoustic stimulation is only oriented along this direction (Figs. 5 and 6).

Using the method presented in Sec. IV B 1, we estimate $A_2$ for each of these four random fields $Z(x)$, as shown in Fig. 11 for $R_F = 42\,\mu$m. We can observe that the linear regressions of both components $Re[u_y]$ and $Im[u_y]$ of the acoustic velocity, were made on the first 5 surface ratios $(1, \frac{1}{4}, \frac{1}{9}, \frac{1}{16}$, and $\frac{1}{25})$ for which the linear approximation expressed in Eq. (23) can be made according to the condition $A \gg A_2$. However, the integral ranges of the two components of the acoustic temperature $\tau$ were estimated from linear regressions on the first 3 surface ratios $(1, \frac{1}{4}$, and $\frac{1}{9})$, which shows that the linear range, for which $A \gg A_2$ is satisfied, is barely reached for our 20 images with surface area equal to $A_C$ (Table I). Larger and more cells $(n \geq 100)$ would give access to a wider linear range for larger surface areas $A$, beyond the values $A_C$ in Table I.

However, the estimated values of $A_2$ of the four acoustic fields are in accordance with the condition $A_C \gg A_2$, since the minimum value of the ratio $A_C/A_2$ is about 100 for $Re[\vec{u}]$, $Im[\vec{u}]$, $Re[\tau]$, and $Im[\tau]$, for the frequency range between 53 Hz and 2095 Hz (Fig. 11).

After having estimated the integral range $A_2$ of each random scalar field ($Re[u_y]$, $Im[u_y]$, $Re[\tau]$, and $Im[\tau]$) for the 20 images (Fig. 11), we can observe its evolution with the frequency of the propagating acoustic wave in the Fig. 12.

Figures 12 and 13 show to what extent the integral range $A_2$ and the relative precision $\epsilon$ in estimating the four average scalar fields decrease when the frequency increases for $R_F = 42\,\mu$m and $R_F = 100\,\mu$m. This can be explained by the relationship which exists between the frequency $f$ and the thickness of the boundary layer $\delta_{BL}$ (Eq. (20)), with $\rho_0$ and $\eta$, respectively, the density and the viscosity of the air filling the pores.[1,2] Moreover, we can observe on Fig. 13 that the maximal relative precision $\epsilon$ of the four scalar fields is about 10%, which is small enough to consider our $n = 20$ simulations as representative for estimating the average harmonic acoustic fields.

#### 2. RVE of the acoustic fields

The representative volume elements $A_{RVE_\epsilon}$ of the four acoustic fields can be estimated from the Eq. (25), which depends on the corresponding integral ranges $A_2$ (Fig. 12). The evolution of $\epsilon$, the precision of estimation of the average acoustic fields is represented in Fig. 14 for different representative volume elements $A_{RVE_\epsilon}$ at different scales and frequencies.

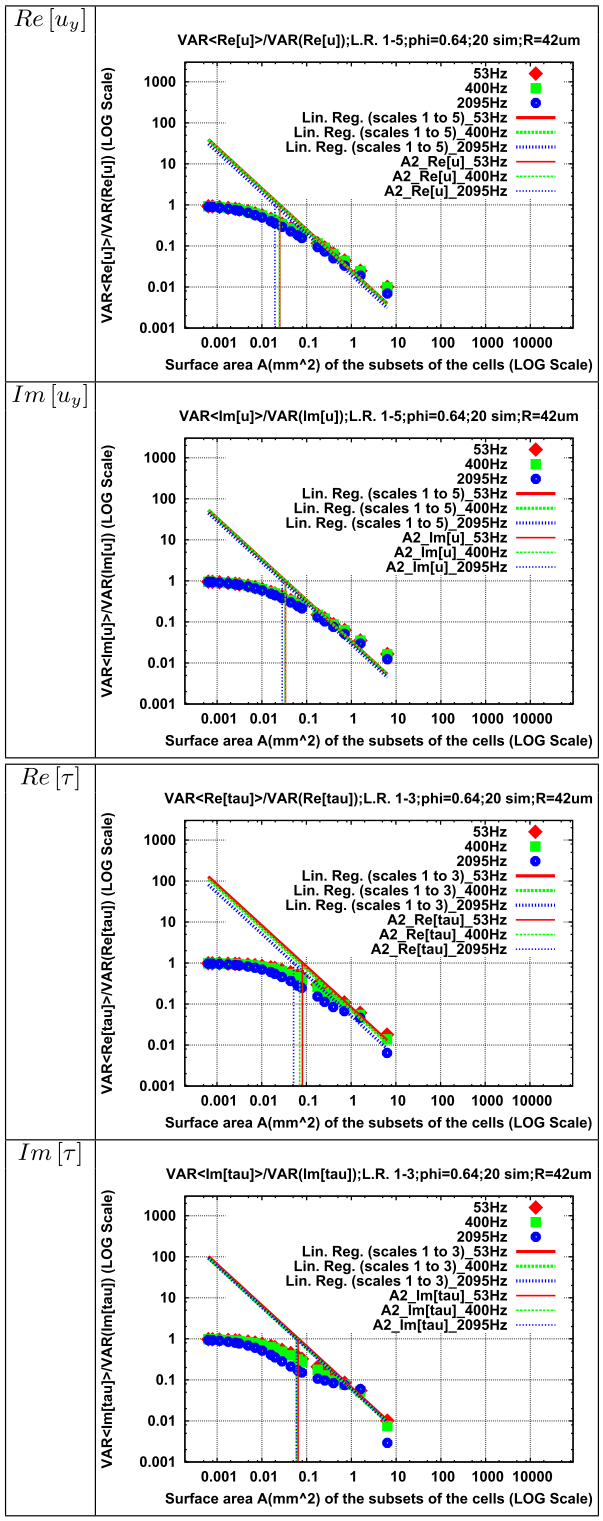


FIG. 11. Estimation of the integral range $A_2$ from linear regressions made on $\frac{VAR(\langle Z\rangle_A)}{VAR(Z)}$ for different frequencies. The variable $Z$ is replaced by $Re[u_y]$, $Im[u_y]$, $Re[\tau]$, and $Im[\tau]$. For both $u_y$ components, the linear regressions are made for the 5 sub-scales $A_C, \frac{A_C}{4}, \frac{A_C}{9}, \frac{A_C}{16}$, *and* $\frac{A_C}{25}$. For both $\tau$ components, the linear regressions are made only for the 3 first sub-scales. $R_F = 42\,\mu$m. Logarithmic scales.

In unit cells composed of small and medium fibres ($R_F = 42\,\mu$m, $100\,\mu$m), we can notice that the values of $A_{RVE_\epsilon}$ decrease at fixed precision $\epsilon$ when the frequency increases (Fig. 14). Therefore, the characteristic sizes of the acoustic

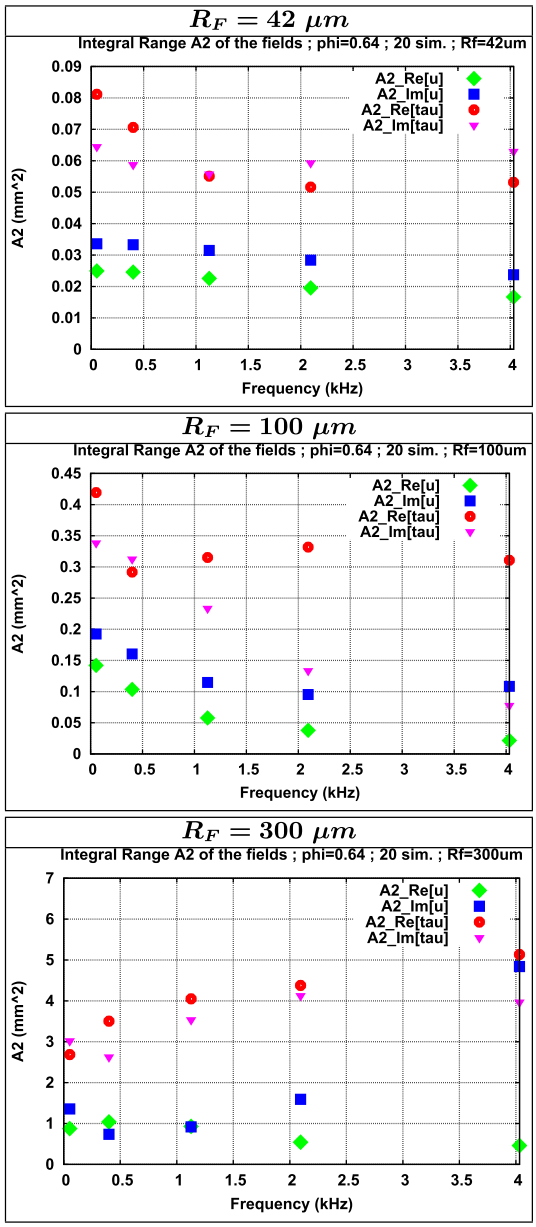


FIG. 12. Evolution of the integral range $A_2$ with $f$ between 53 Hz and 4032 Hz for $Re[u_y]$, $Im[u_y]$, $Re[\tau]$, and $Im[\tau]$, at different scales ($R_F = 42\,\mu$m, $100\,\mu$m, and $300\,\mu$m).

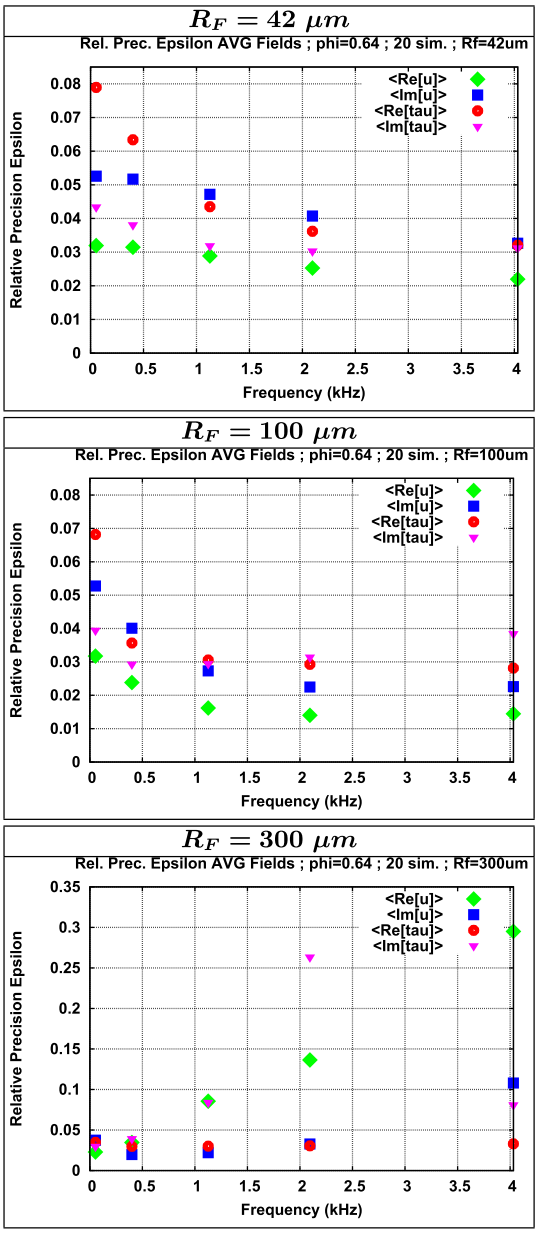


FIG. 13. Evolution of the relative precision of estimation $\epsilon$ with $f$ between 53 Hz and 4032 Hz for $\langle Re[u_y]\rangle$, $\langle Im[u_y]\rangle$, $\langle Re[\tau]\rangle$, and $\langle Im[\tau]\rangle$, at different scales ($R_F = 42\,\mu$m, $100\,\mu$m, and $300\,\mu$m). The relative precision was obtained with $n = 20$ independent simulations with a surface area equal to $A_C$ (Table I).

fields in unit cells are smaller at high frequencies for $R_F = 42\,\mu$m and $R_F = 100\,\mu$m, which is consistent with the decrease of the thickness of the boundary layer at high frequencies (Eq. (20)), giving fields with a lower correlation length.

However, the representative volume elements $A_{RVE_\epsilon}$ of the fields obtained from cells with large fibres ($R_F = 300\,\mu$m) do not seem to evolve with the same monotonic trend as for smaller fibres.

### D. Representative volume element of the acoustic absorption

#### 1. Relative precision in the estimation of the acoustic absorption

In order to estimate the relative precision $\epsilon$ of estimation of the acoustic absorption with the Eq. (24), the integral range $A_2$ cannot be estimated, since there is no point variance $VAR(Z)$ for $\alpha(\omega)$. However, we can estimate the product $VAR(Z) \times A_2$ with a linear regression of $VAR(\langle Z\rangle_A)$ as a function of $1/A$ (Eq. (23)). Thus, using this linear regression and the Eq. (24), we obtained the precision $\epsilon$ of the acoustic absorption as a function of the total surface area $A_0 = n \times A_C$ of our 20 simulations.

The frequential evolution of $\epsilon$ is represented in Fig. 15. We can observe that all the values of $\epsilon$ are globally smaller than 5% and smaller than the precision of estimation of the average acoustic fields (Fig. 13) for $R_F = 42\,\mu$m and $R_F = 100\,\mu$m. Moreover, the values of $\epsilon$ decrease when both the thickness $d$ of the material and the frequency increase, for small and medium fibres ($R_F = 42\,\mu$m and $100\,\mu$m).

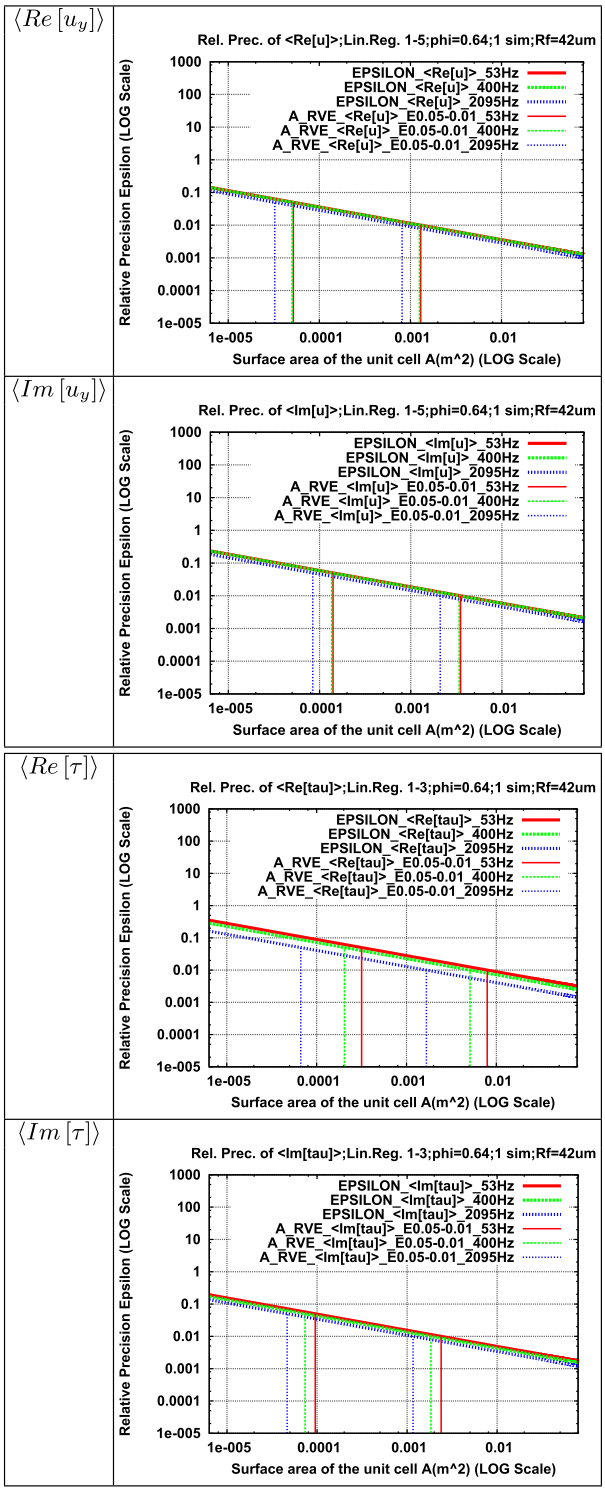


FIG. 14. Evolution of the relative precision of estimation $\epsilon$ of $\langle Re[u_y]\rangle$, $\langle Im[u_y]\rangle$, $\langle Re[\tau]\rangle$, and $\langle Im[\tau]\rangle$ over the surface area $A$ of one random realization (n = 1) for $R_F = 42\,\mu$m. The minimum surface area $A$ on the $Ox$ axis is equal to $A_C$ in Table I. Interval between two colored dashed vertical lines: $\epsilon \in [1\% - 5\%]$. Logarithmic scales.

For large fibres ($R_F = 300\,\mu$m) the fluctuations and the 95% confidence interval previously observed in Fig. 7 are direct consequences of the high values of $\epsilon$ for the acoustic absorption. This results show that the size $A_C$ of the 20 simulations (Table I) is probably not large enough to properly quantify the fluctuation of the acoustic absorption of large

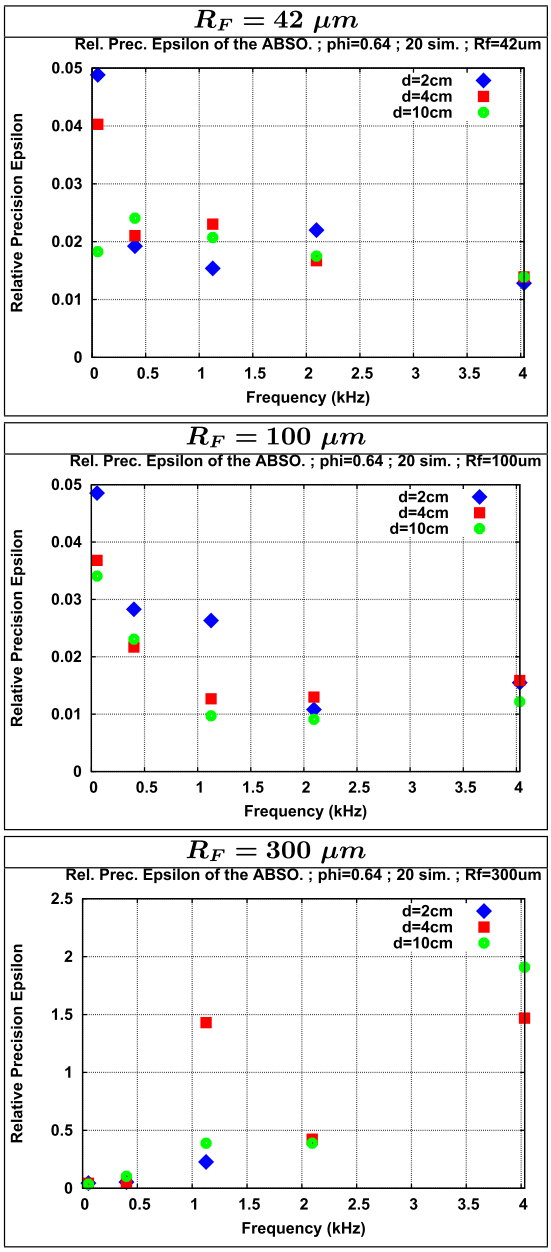


FIG. 15. Evolution of the relative precision $\epsilon$ with $f$ between 53 Hz and 4032 Hz for the absorption coefficient $\alpha(\omega)$, at different scales ($R_F = 42\,\mu$m, 100 $\mu$m, and 300 $\mu$m) and for different thicknesses ($d = 2$ cm, 4 cm, and 10 cm). The relative precision was obtained with $n = 20$ independent simulations with a surface area equal to $A_C$ (Table I).

fibres, even if the average value of $\alpha(\omega)$ of the 20 realizations is not very different from the absorption obtained on a deterministic fibre network (orange plots in Fig. 7).

### 2. RVE of the acoustic absorption

Finally, the last step of our work consists in estimating the representative volume element for the acoustic absorption. In Fig. 16, we can observe the evolution of the relative precision of estimation $\epsilon$ of the average value $E\{\alpha(\omega)\}$ with the size $A$ of one simulation of random fibrous media. As a consequence of the results obtained for the acoustic fields (Fig. 14), the relative error $\epsilon$ monotonically decreases (giving a better precision) when the frequency increases for small

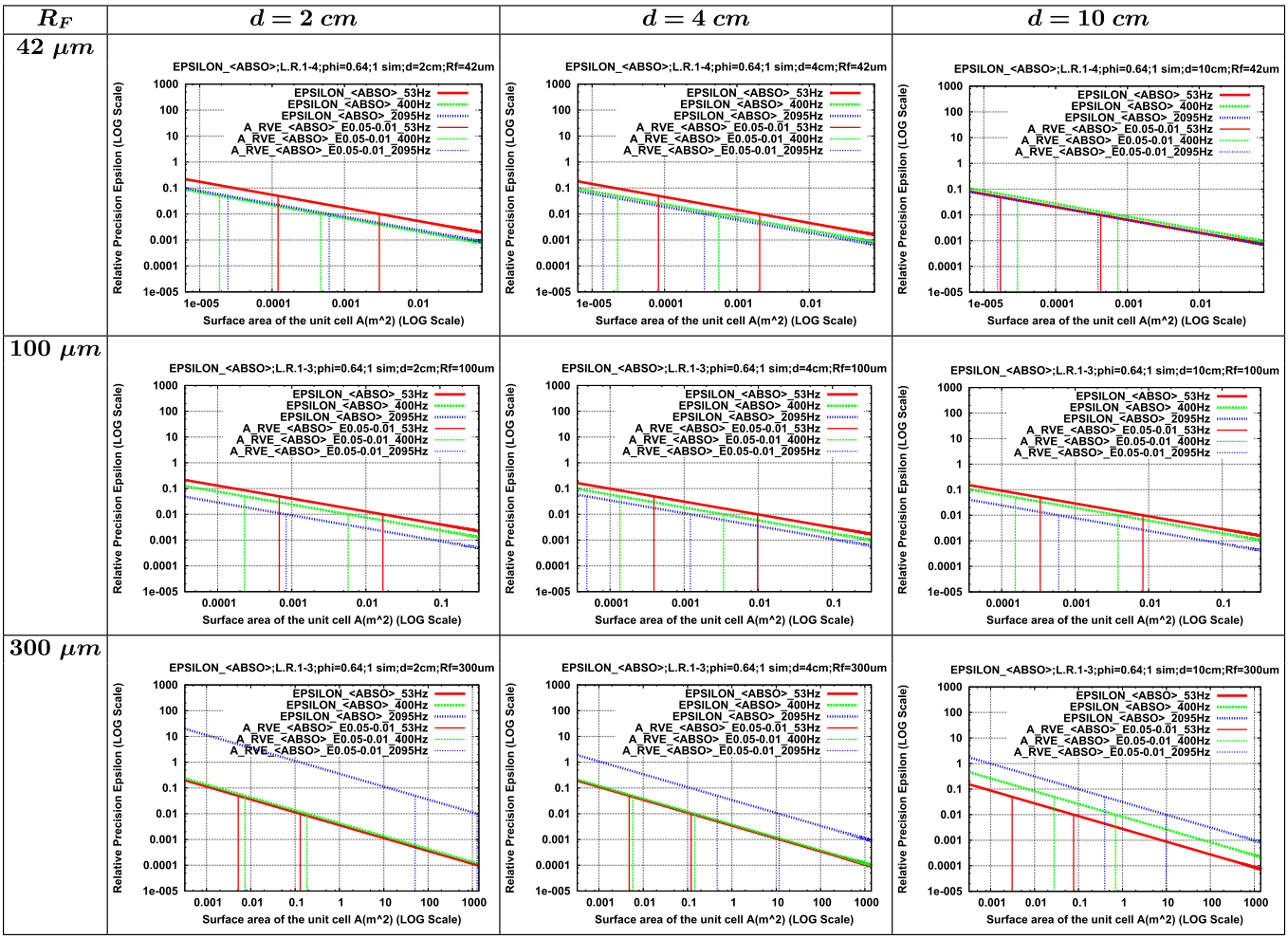


FIG. 16. Evolution of the relative precision of estimation $\epsilon$ of the average acoustic absorption $E\{\alpha(\omega)\}$ over the surface area $A$ of one random realization (n = 1) at different scales ($R_F = 42\,\mu$m, $100\,\mu$m, and $300\,\mu$m), for thicknesses $d$ equal to 2 cm, 4 cm, and 10 cm, and for $f$ between 53 Hz and 2095 Hz. The minimum surface area $A$ on the $Ox$ axis is equal to $A_C$ in Table I. Interval between two colored dashed vertical lines: $\epsilon \in [1\% - 5\%]$. Logarithmic scales.

and medium fibres ($R_F = 42\,\mu$m, $100\,\mu$m), for the three considered thicknesses ($d = 2$ cm, 4 cm, and 10 cm). This is a direct effect of the frequential evolution of the thickness $\delta_{BL}$ of the boundary layer (Eq. (20)). This trend is not observable for large fibres ($R_F = 300\,\mu$m).

Let us focus on the precision of estimation of $E\{\alpha(\omega)\}$ over a single simulation composed of small and medium fibres ($R_F = 42\,\mu$m, $100\,\mu$m) with a surface area equal to $A_C$ (Table I). Even if the maximal value of $\epsilon$ is equal to 20% at low frequencies ($f = 53$ Hz), the values of the precision are close to 10% for frequencies higher than 400 Hz (Fig. 16). Therefore, we observe that one unit cell with a surface area equal to $A_C$ is representative enough to estimate the average absorption coefficient with a precision of 10%, over the frequency range between 53 Hz and 2095 Hz. This gives the size of the domain to be used in the random network, to estimate the effective acoustic properties with a given precision.

## V. CONCLUSIONS

Estimating the acoustic behaviour of random media is a challenging problem, which was recently developed by numerical techniques on images of the microstructure. In this paper is considered the effect of the size of fibres and of their random distribution in space on the acoustic behaviour.

Following a method efficiently applied in the domains of elastostatics and of thermostatics,[4,13,17,19,43] we extended the statistical determination of the RVE to the harmonic case, in the framework of thermoacoustics. As a result, we are able to estimate the relative precision of estimation of the acoustic properties of porous media, predicted from numerical simulations of the complex harmonic velocity and temperature fields in a random medium submitted to an acoustic wave propagation. This precision depends on the scale of calculations, and on the local fluctuations of the fields that can be estimated by numerical techniques. In the present case, thermal properties fluctuate more and develop longer correlation lengths than velocity fields. The thermal properties are therefore the limiting factor to define a representative volume element. The effect of the frequency is to decrease the size of the RVE, as a result of the thinning of the boundary layer giving more localized fields.

The method illustrated here on a random fibrous medium can be used on more general 3D images or simulations, like foams or granular media, provided the corresponding fields are obtained by numerical calculation.

## ACKNOWLEDGMENTS

This work was made as a part of the Silent Wall project (Ref.: ANR-06-MAPR-00-18). We gratefully acknowledge the Agence Nationale de la Recherche (ANR) for its financial support. Moreover, we are grateful to Bernard Castagnède, Claude Depollier and Olivier Dazel (LAUM, Laboratoire d'Acoustique de l'Université du Maine, Le Mans, France) for bringing their expert's point of view in acoustics all along this project.

[1]J. F. Allard, *Propagation of Sound in Porous Media. Modelling Sound Absorbing Materials* (Chapman & Hall, London, 1993).
[2]J. F. Allard, B. Castagnède, M. Henry, and W. Lauriks, "Evaluation of tortuosity in acoustic porous materials saturated by air," Rev. Sci. Instrum. **65**, 754–755 (1994).
[3]J. F. Allard and Y. Champoux, "New empirical equations for sound propagation in rigid frame fibrous materials," J. Acoust. Soc. Am. **91**(6), 3346–3353 (1992).
[4]H. Altendorf, "3D Morphological analysis and modeling of random fiber networks," Ph.D. thesis, Mines ParisTech, 2011.
[5]J. L. Auriault, "Dynamic behaviour of a porous medium saturated by a Newtonian fluid," Int. J. Eng. Sci. **18**(6), 775–785 (1980).
[6]J. L. Auriault, L. Borne, and R. Chambon, "Dynamics of porous saturated media, checking of the generalized law of Darcy," J. Acoust. Soc. Am. **77**(5), 1641–1650 (1985).
[7]J. L. Auriault and E. Sanchez-Palencia, "Étude du comportement macroscopique d'un milieu poreux saturé déformable," J. de Mécanique **16**(4), 575–603 (1977).
[8]Y. Champoux and J. F. Allard, "Dynamic tortuosity and bulk modulus in air-saturated porous media," J. Appl. Phys. **70**(4), 1975–1979 (1991).
[9]Y. Champoux and M. R. Stinson, "On acoustical models for sound propagation in rigid frame porous materials and the influence of shape factors," J. Acoust. Soc. Am. **92**(2), 1120–1131 (1992).
[10]A. M. Chapman and J. J. L. Higdon, "Oscillatory Stokes flow in periodic porous media," Phys. Fluids A **4**(10), 2099–2116 (1992).
[11]Comsol Multiphysics™ 3.5a, *Comsol Multiphysics™ 3.5a-Documentation*, http://www.comsol.com/, 2009.
[12]M. E. Delany and E. N. Bazley, "Acoustical properties of fibrous absorbent materials," Appl. Acoust. **3**, 105–116 (1970).
[13]J. Escoda, F. Willot, D. Jeulin, J. Sanahuja, and C. Toulemonde, "Estimation of local stresses and elastic properties of a mortar sample by FFT computation of fields on a 3D image," Cem. Concr. Res. **41**, 542–556 (2011).
[14]S. Gasser, "Étude des propriétés acoustiques et mécaniques d'un matériau métallique poreux modèle base de sphères creuses de nickel," Ph.D. thesis, INPG Grenoble, 2003.
[15]S. Gasser, F. Paun, and Y. Bréchet, "Absorptive properties of rigid porous media: Application to face centered cubic sphere packing," J. Acoust. Soc. Am. **117**, 2090–2099 (2005).
[16]D. Jeulin, "Random texture models for materials structures," Stat. Comput. **10**, 121–131 (2000).
[17]D. Jeulin, "Variance scaling of boolean random varieties," Technical report, Mines ParisTech Publications-HAL-00618967, 2011.
[18]D. L. Johnson, J. Koplik, and R. Dashen, "Theory of dynamic permeability and tortuosity in fluid-saturated porous media," J. Fluid Mech. **176**, 379–402 (1987).
[19]T. Kanit, S. Forest, I. Galliet, V. Mounoury, and D. Jeulin, "Determination of the size of the representative volume element for random composites: Statistical and numerical approach," Int. J. Solids Struct. **40**, 3647–3679 (2003).
[20]D. Lafarge, "Propagation du son dans les matériaux poreux structure rigide saturés par un fluide viscothermique," Ph.D. thesis, University of the Maine, 1993.
[21]C. Y. Lee, M. J. Leamy, and J. H. Nadler, "Numerical calculation of effective density and compressibility tensors in periodic porous media: A multiscale asymptotic method," in Proceedings of the COMSOL Conference, Boston, USA, 9–11 October 2008.
[22]C. Y. Lee, M. J. Leamy, and J. H. Nadler, "Acoustic absorption calculation in irreducible porous media: A unified computational approach," J. Acoust. Soc. Am. **126**(4), 1862–1870 (2009).
[23]G. Matheron, *Éléments pour une Théorie des Milieux Poreux* (Masson, Paris, 1967).
[24]G. Matheron, "The theory of regionalized variables and its applications," Technical report, Mines ParisTech Publications, 1971.
[25]F. P. Mechel, "Ausweitung der absorberformel von delany and bazley zu tiefen frequenzen," Acustica **35**, 210–213 (1976).
[26]Y. Miki, "Acoustical properties of porous materials-generalizations of empirical models," J. Acoust. Soc. Jpn. (E) **11**(1), 25–28 (1990).
[27]Y. Miki, "Acoustical properties of porous materials-modifications of Delany-Bazley models," J. Acoust. Soc. Jpn. (E) **11**(1), 19–24 (1990).
[28]C. Perrot, "Microstructure et macro-comportement acoustique: approche par reconstruction d'une cellule élémentaire représentative," Ph.D. thesis, University of Sherbrooke; ENTPE Lyon, 2006.
[29]C. Perrot, F. Chevillotte, M. T. Hoang, G. Bonnet, F. X. Bécot, L. Gautron, and A. Duval, "Microstructure, transport, and acoustic properties of open-cell foam samples: Experiments and three-dimensional numerical simulations," J. Appl. Phys. **111**, 014911 (2012).
[30]C. Perrot, F. Chevillotte, and R. Panneton, "Bottom-up approach for microstructure optimization of sound absorbing materials," J. Acoust. Soc. Am. **124**, 940–948 (2008).
[31]C. Perrot, F. Chevillotte, and R. Panneton, "Dynamic viscous permeability of an open-cell aluminium foam: Computation versus experiments," J. Appl. Phys. **103**, 024909 (2008).
[32]C. Peyrega, "Prediction of the acoustic properties of heterogeneous fibrous materials from their 3D microstructures," Ph.D. thesis, Mines ParisTech, 2010.
[33]C. Peyrega and D. Jeulin, "Effects of the microstructure of fibrous media on their acoustic properties," in Proceedings of the COMSOL Conference, Versailles, France, 17th–19th November 2010.
[34]C. Peyrega and D. Jeulin, "Simulation of the acoustic behaviour of random fibrous materials," in Proceedings of the Internoise Conference, Osaka, Japan, 4th–7th September 2011.
[35]C. Peyrega, D. Jeulin, C. Delisée, and J. Malvestio, "3D morphological modelling of a random fibrous network," Image Anal. Stereol. **28**, 129–141 (2009).
[36]C. Peyrega, D. Jeulin, C. Delisée, and J. Malvestio, "3D morphological characterization of phonic insulation fibrous media," Adv. Eng. Mater. **13**(3), 156–164 (2010).
[37]J. Pfretzschner and R. M. Rodríguez, "Acoustical absorption and critical thickness," in Proceedings of the 17th International Congress of Acoustics (ICA) 2001, Rome, Italie, 2–7 September 2001.
[38]S. R. Pride, F. D. Morgan, and A. F. Gangi, "Drag forces of porous media acoustics," Phys. Rev. B **47**(9), 4964–4975 (1993).
[39]E. Sanchez-Palencia, "Comportements local et macroscopique d'un type de milieux physiques hétérogènes," Int. J. Eng. Sci. **12**(4), 331–351 (1974).
[40]E. Sanchez-Palencia, *Non-Homogeneous Media and Vibration Theory* (Springer-Verlag, Heidelberg, 1980).
[41]R. Venegas and O. Umnova, "On the influence of the micro-geometry on sound propagation through periodic array of cylinders," in Proceedings of Acoustics 08, Paris, France, 29th June–4th July 2008, pp. 807–812.
[42]R. Venegas and O. Umnova, "Effective acoustical properties of random microfibrous materials," in Proceedings of Euronoise 2009, Edinburgh, Scotland, 26th–28th October 2009.
[43]F. Willot and D. Jeulin, "Elastic behavior of composites containing boolean random sets of inhomogeneities," Int. J. Eng. Sci. **47**, 313–324 (2009).
[44]C. Zwikker and C. W. Kosten, *Sound Absorbing Materials* (Elsevier applied sciences, New-York, 1949).